AIAA JOURNAL
Vol. 32, No. 10, October 1994

Unsteady Supersonic Cavity Flow Simulations Using Coupled k-ε and Navier-Stokes Equations

S. H. Shih,* A. Hamed,† and J. J. Yeuan‡
University of Cincinnati, Cincinnati, Ohio 45221

A numerical procedure is developed for the simultaneous implicit numerical solution of the coupled k-ε and Navier-Stokes equations for compressible viscous flows. The numerical algorithm is based on the approximate factorization scheme of Beam and Warming for the strongly coupled set of equations. The scheme incorporates a new second-order Jameson type damping model that enhances the stability and relieves the stiffness associated with the solution to the k-ε equations. The model, which is based on the changes in both pressure and turbulent kinetic energy, eliminates the need to use subiteration techniques. Unsteady calculations were performed for supersonic flow over an open cavity at a freestream Mach number of 1.5 and Reynolds number of 1.09×10^6. The computed results are compared with experiments and predictions from computations using uncoupled k-ε and Navier-Stokes equations.

Nomenclature

E	= total energy
J	= Jacobian of coordinate transformation
k	= turbulent kinetic energy
P	= static pressure
t	= time
u, v	= Cartesian velocities
x, y	= Cartesian coordinates
ε	= turbulent dissipation rate
ξ, η	= curvilinear coordinates
ρ	= density

Introduction

SUPERSONIC flows over open cavities can produce complex unsteady flowfields involving self-induced pressure oscillations, and periodic mass addition and expulsion from the cavity. The intense pressure fluctuations and severe acoustic environment can be of importance in terms of the structural integrity of aerodynamic performance and stability of supersonic aircrafts. Some understanding of the complex interaction between the external shear layer and cavity acoustical disturbances has been achieved through experimental, analytical, and numerical studies.[1–5] Modeling the fluctuating shear layers, the traversing pressure waves inside and the oblique shock waves outside the cavity is very critical in these flows. Numerical solutions of the compressible unsteady Navier-Stokes equations with algebraic turbulence models were obtained by Hankey and Shang[4] and Rizzetta.[5] Even through the two-equation turbulence models[7–13] have been used extensively with the Navier-Stokes equations for the numerical simulations of compressible viscous flows, they have not been applied to the supersonic cavity problem. Rizzetta and Visbal[14] have used a two-equation turbulence model in the unsteady flow simulations around a pitching airfoil. Their approach required subiteration with fractional time steps in the solution of the k and ε equations. The present investigation is focused on the development of an appropriate numerical procedure to couple the Navier-Stokes and k-ε equations for unsteady flow simulation. The proposed time-dependent full Navier-Stokes algorithm with a two-equation turbulence model is based on the Beam and Warming approximate factorization implicit scheme. Since the governing equations for the mean flow and turbulence quantities are integrated simultaneously at each time step, the scheme does not suffer from the frequency spectrum problem discussed by Hankey and Calarese.[6] A new Jameson type damping model, in which the second-order terms are based on the changes in both the pressure and the turbulent kinetic energy, is proposed and used in the unsteady two-dimensional simulations of the supersonic cavity flow.

Presented as Paper 93-3031 at the AIAA 24th Fluid Dynamics Conference, Orlando, FL, July 6–9, 1993; received Sept. 28, 1993; revision received May 10, 1994; accepted for publication May 16, 1994.

*Graduate Research Assistant, Department of Aerospace Engineering and Engineering Mechanics. Student Member AIAA.

†Professor, Department of Aerospace Engineering and Engineering Mechanics. Fellow AIAA.

‡Postdoctoral Assistant, Department of Aerospace Engineering and Engineering Mechanics. Member AIAA.

Governing Equations

The governing equations in general curvilinear coordinates are written in terms of the mass-averaged variables for the strongly coupled Navier-Stokes equations and two-equation turbulence model.[15]

$$\frac{\partial U}{\partial t} + \frac{\partial E}{\partial \xi} + \frac{\partial F}{\partial \eta} = \frac{\partial V_1}{\partial \xi} + \frac{\partial V_2}{\partial \xi} + \frac{\partial W_1}{\partial \eta} + \frac{\partial W_2}{\partial \eta} + H \tag{1}$$

where

$$U = 1/J\,[\rho, \rho u, \rho v, \rho E, \rho k, \rho \varepsilon]^T \tag{2}$$

where E and F are inviscid fluxes, and V_1, V_2, W_1, and W_2 are viscous fluxes. In the equations, all variables were normalized by their respective freestream values except for the pressure, which was nondimensionalized by the freestream dynamic pressure. The matrix H contains the source terms (production and dissipation), which come from the turbulence equations. The detailed description of the governing equations can be found in Ref. 15. The turbulence model is based on Chien's low Reynolds number two-equation turbulence model[11] modified by Nichols[12] to account for the compressibility effects and irrotational strain. The Sutherland law for the molecular viscosity coefficient and the perfect gas relationship were also employed.

Numerical Procedure

Applying the Beam-Warming's implicit approximate factorization finite difference scheme[16] to the governing equations leads to block tridiagonal systems of equations.

$$\left\{ I + \frac{\theta_1 \Delta t}{1 + \theta_2} \left[\frac{\partial A^n}{\partial \xi} - \frac{\partial^2 R^n}{\partial \xi^2} + \frac{\partial B^n}{\partial \eta} - \frac{\partial^2 S^n}{\partial \eta^2} - D^n \right] \right\} \Delta^n U$$

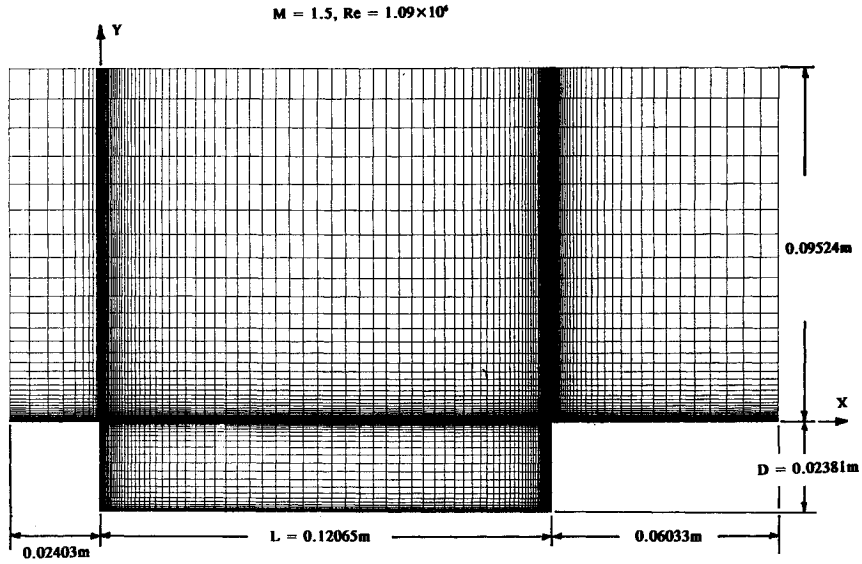

Fig. 1 Solution domain and computational grid for supersonic flow over an open cavity.

$$= \frac{\Delta t}{1+\theta_2}\left[\frac{\partial}{\partial\xi}(-E^n + V_1^n + V_2^n) + \frac{\partial}{\partial\eta}(-F^n + W_1^n + W_2^n) + H^n\right]$$

$$+ \frac{\theta_1 \Delta t}{1+\theta_2}\left[\frac{\partial}{\partial\xi}(\Delta^{n-1} V_2) + \frac{\partial}{\partial\eta}(\Delta^{n-1} W_1)\right] \frac{\theta_2}{1+\theta_2}\Delta^{n-1} U \qquad (3)$$

where

$$\Delta^n U = U^{n+1} - U^n \qquad (4)$$

Near the wall, the turbulence source terms (production and dissipation) can be very large compared to the convective terms leading to a stiff algorithm if the turbulence source terms are treated explicitly.[7–10] The inclusion of the Jacobian matrix D in the implicit part is necessary to balance the explicit turbulence source term on the right-hand side of Eq. (3). The Jacobian matrices A, B, R, S, and D are given by

$$A = \frac{\partial E}{\partial U}, \quad B = \frac{\partial F}{\partial U}, \quad D = \frac{\partial H}{\partial U}, \quad R = \frac{\partial V_1}{\partial U_\xi}, \quad S = \frac{\partial W_2}{\partial U_\eta} \qquad (5)$$

In two-dimensional flows, the present algorithm results in 6×6 Jacobian matrices A, B, D, R, and S whose elements are given by

$$a_{ij} = \frac{\partial E_i}{\partial q_j}, \quad b_{ij} = \frac{\partial F_i}{\partial q_j}, \quad d_{ij} = \frac{\partial H_i}{\partial q_j}$$

$$r_{ij} = \frac{\partial V_{1i}}{\partial q_{j,\xi}}, \quad s_{ij} = \frac{\partial W_{2i}}{\partial q_{j,\eta}} \qquad (6)$$

where both the mean flow and turbulence quantities are included in the vector of

$$q_1 = \rho/J, \quad q_2 = \rho u/J, \quad q_3 = \rho v/J$$

$$q_4 = \rho E/J, \quad q_5 = \rho k/J, \quad q_6 = \rho \varepsilon/J \qquad (7)$$

The subscripts ,ξ and ,η in Eq. (6) represent the partial derivatives with respect to ξ and η. The difference formula, Eq. (3), is approximately factored as follows:

$$\left\{I + \frac{\theta_1 \Delta t}{1+\theta_2}\left[\frac{\partial A^n}{\partial\xi} - \frac{\partial^2 R^n}{\partial\xi^2} - D^n\right]\right\}$$

$$\times \left\{I + \frac{\theta_1 \Delta t}{1+\theta_2}\left[\frac{\partial B^n}{\partial\eta} - \frac{\partial^2 S^n}{\partial\eta^2}\right]\right\} = \text{rhs [Eq. (3)]} \qquad (8)$$

The governing equations are integrated simultaneously at each time step with no time lag between the mean flow and turbulence quantities. The three-point backward implicit scheme ($\theta_1 = 1$, $\theta_2 = 1/2$) that is second-order accurate in time is used in the present study. The turbulent source terms are coupled not only with the turbulent quantities but also with the mean flow fluxes. All spatial derivatives were approximated by second-order accurate central differences. To prevent even-odd numerical oscillations, common forms of fourth-order and second-order artificial dissipation[16] were employed to maintain numerical stability. In the turbulence equations, convection terms often dominate the diffusion in the far field (away from the wall) and can cause convective instability, leading to oscillations of the turbulence field variables near the boundary-layer edge. The following second-order dissipation based on the changes of both pressure and turbulent kinetic energy is postulated:

$$D_\xi = \frac{1}{4p}\left|\frac{\partial^2 p}{\partial\xi^2}\right| + \frac{1}{4k}\left|\frac{\partial^2 k}{\partial\xi^2}\right|, \qquad D_\eta = \frac{1}{4p}\left|\frac{\partial^2 p}{\partial\eta^2}\right| + \frac{1}{4k}\left|\frac{\partial^2 k}{\partial\eta^2}\right| \qquad (9)$$

Figure 1 shows the solution domain and computational grid. The inflow boundary conditions are obtained from the numerical solution of the steady flow over a flat plate at the freestream conditions of the cavity flow. The flat plate computational domain extends from the leading edge to 0.19916 times the cavity length upstream of the cavity forward bulkhead to establish the upstream profiles.

A turbulent intensity level T_i, defined as

$$T_i = \left(\frac{2}{3}k_\infty\right)^{1/2}/u_\infty \qquad (10)$$

was set to 0.005 (Ref. 14) in the freestream to prescribe the magnitude of the turbulent kinetic energy. Corresponding values of the freestream dissipation were then determined by requiring that eddy viscosity is equal to the freestream molecular viscosity. Initial conditions are taken as the flat plate profile at all grid locations lying above the cavity mouth. For the grid points within the cavity, wall values are assigned.

At the solid surfaces, the no-slip and adiabatic wall conditions are applied with vanishing normal pressure gradient. The turbulent variables k and ε are equal to zero at the wall due to inclusion of the low-Reynolds number terms in the k-ε equations. In the far field, derivatives along the instantaneous Mach lines were set to

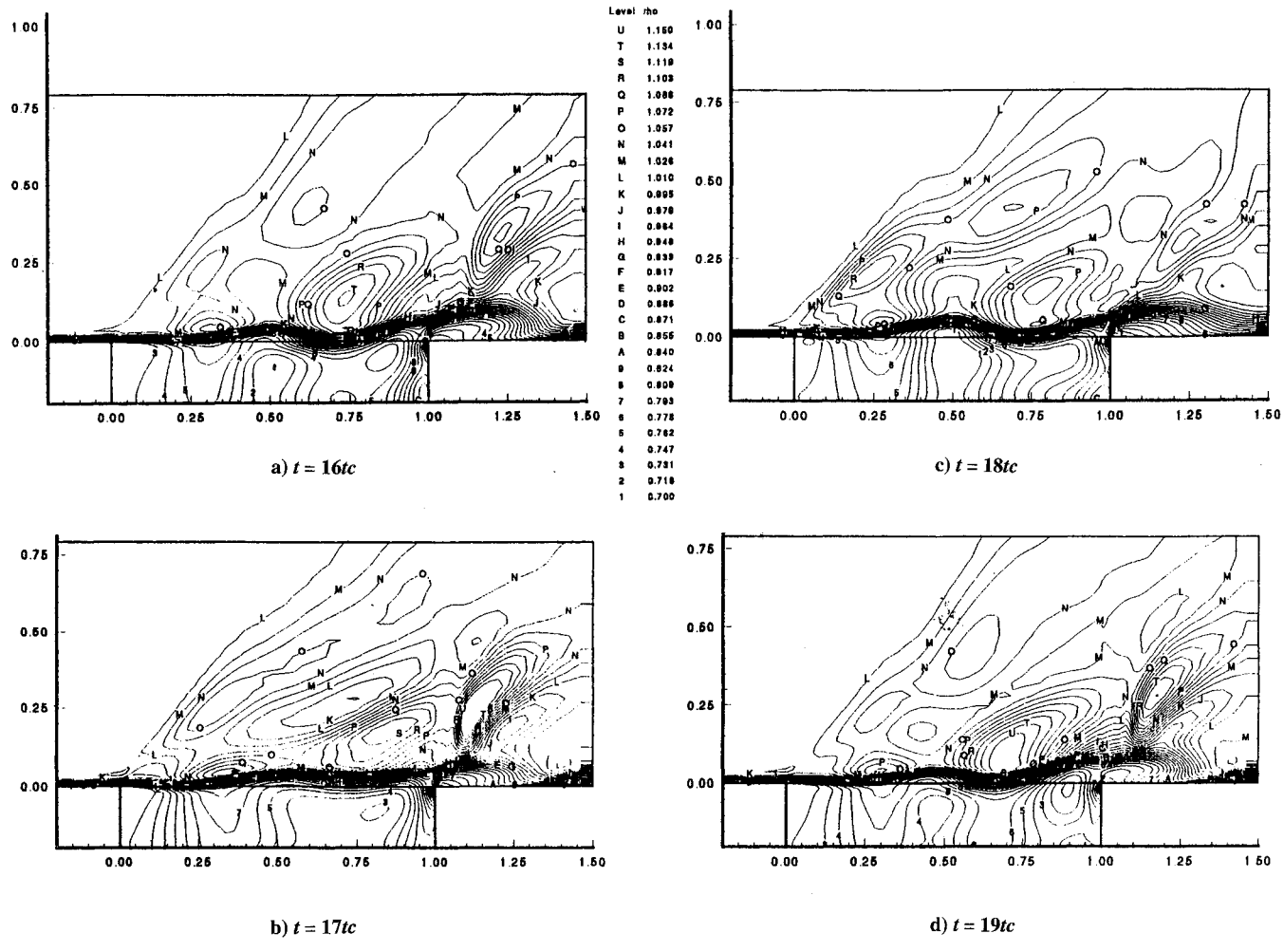

Fig. 2 Instantaneous density contours.

zero, which had previously proven successful in other computations.[4,5] This condition was expressed as follows:

$$(\xi_x + \xi_y \tan\theta)\frac{\partial U}{\partial \xi} + (\eta_x + \eta_y \tan\theta)\frac{\partial U}{\partial \eta} = 0 \qquad (11)$$

where $\theta = \arcsin(1/M)$ and M is the local Mach number. Along the outflow boundary, first-order accurate extrapolation of all dependent variables was employed.

Results and Discussions

Unsteady supersonic flow simulations over an open cavity were conducted for one of the cases from the comprehensive experimental study of Kaufman et al.[1] The experiments were conducted in the Air Force Wright Aeronautical Laboratory at a freestream Mach number of 1.5 and the Reynolds number of 1.09×10^6, based on freestream conditions and the cavity length. Referring to Fig. 1, the cavity has a length-to-depth ratio of 5.07 with length L of 0.12065 m, depth D of 0.02381 m, and width W of 0.0635 m. In the present study, the numerical solution is obtained for flow over a two-dimensional cavity, and the results are compared with the experimental data along the cavity's midspan. It was verified, experimentally[1,2] and computationally,[5] that the fundamental behavior of the oscillations is two dimensional.

The computational grid shown in Fig. 1 consists of 150×51 points on and above the plane of the cavity mouth and 96×40 points inside the cavity. This distribution employed 15 x-grid points upstream of the forward bulkhead and 41 points downstream of the aft bulkhead. The overall extent of the domain was 0.19916 of cavity length upstream and 1.5 of cavity length downstream of the forward bulkhead, and four times of the cavity depth above the plane of cavity mouth. Simple exponential stretching was used to cluster the grid lines at all solid boundaries and at the plane of the cavity mouth. The minimum grid spacings in the streamwise and normal directions were 3.62×10^{-4} and 5.86×10^{-5} of the cavity length, respectively, resulting in a value of $y^+ = 1.5$ at the first mesh point above the plane of the mouth. This grid distribution with approximately 28 points within the incoming boundary layer was considered to be adequate for the shear-layer resolution downstream.

Starting from the initial profiles, the flowfield solution was integrated in time using the three-point backward implicit scheme, which is second-order accurate in time. For the present code, the time step size was 2.5×10^{-4} corresponding to a maximum local Courant-Fredericks-Lewy (CFL) number of 420 for stability consideration. After 16,000 time steps, corresponding to 4.0 characteristic times ($u_{\text{inf}}t/L$), it was judged that the flowfield had been purged of initial transients and the oscillations were self-sustaining. The time-dependent simulations for 64,000 time steps corresponding to 16.0 characteristic times were used to produce the presented results for comparisons with the experimental measurements. The entire computation required approximately 20 CPU h on the Cray Y-MP.

Figures 2 and 3 present the instantaneous density and pressure contours obtained from the present code at four different time levels. These figures demonstrate the shear-layer fluctuations, causing periodic mass addition and expulsion from the cavity. The shear-layer deflection causes an extremely complex flowfield,

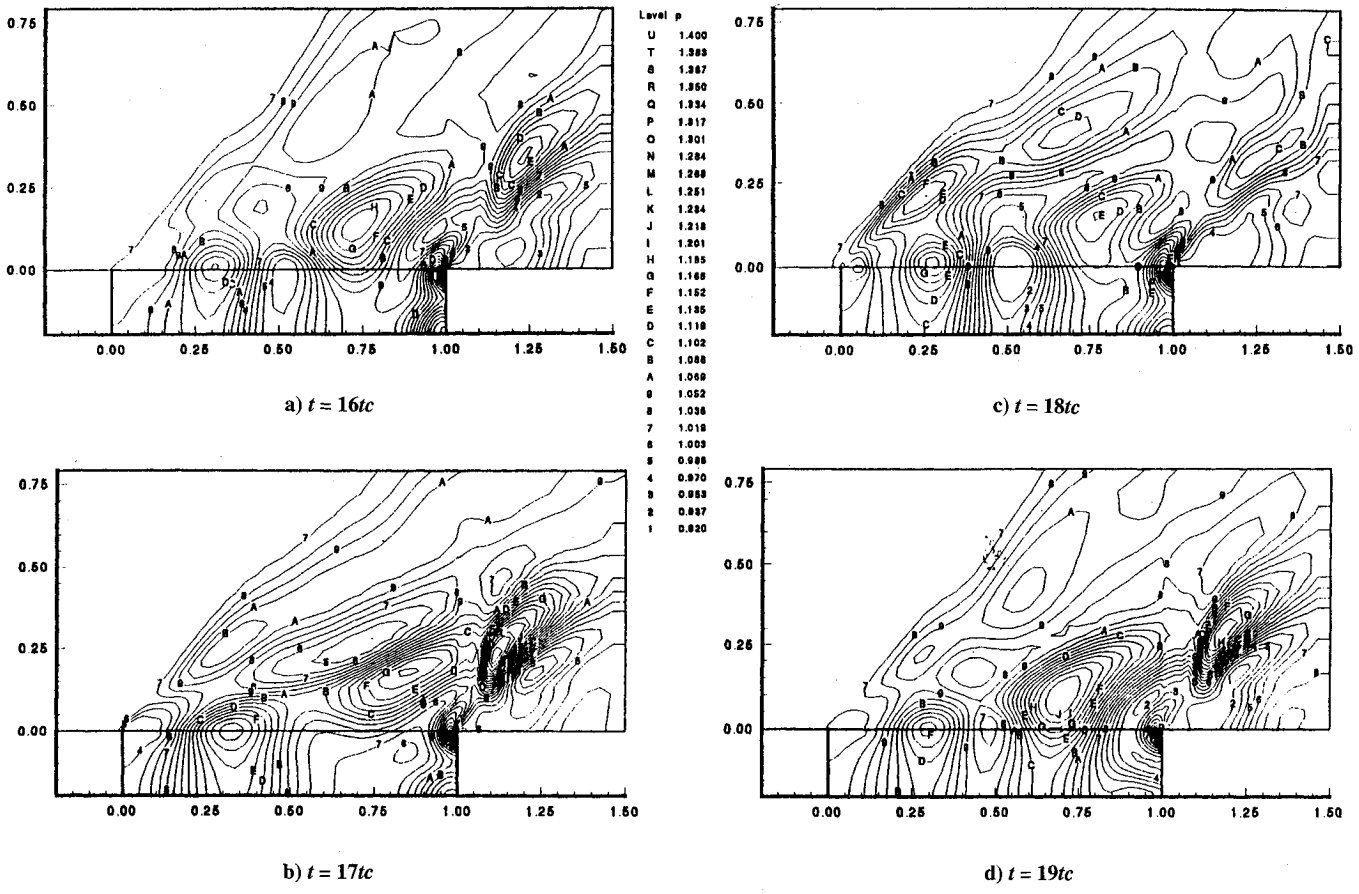

a) $t = 16tc$

c) $t = 18tc$

b) $t = 17tc$

d) $t = 19tc$

Fig. 3 Instantaneous static pressure contours.

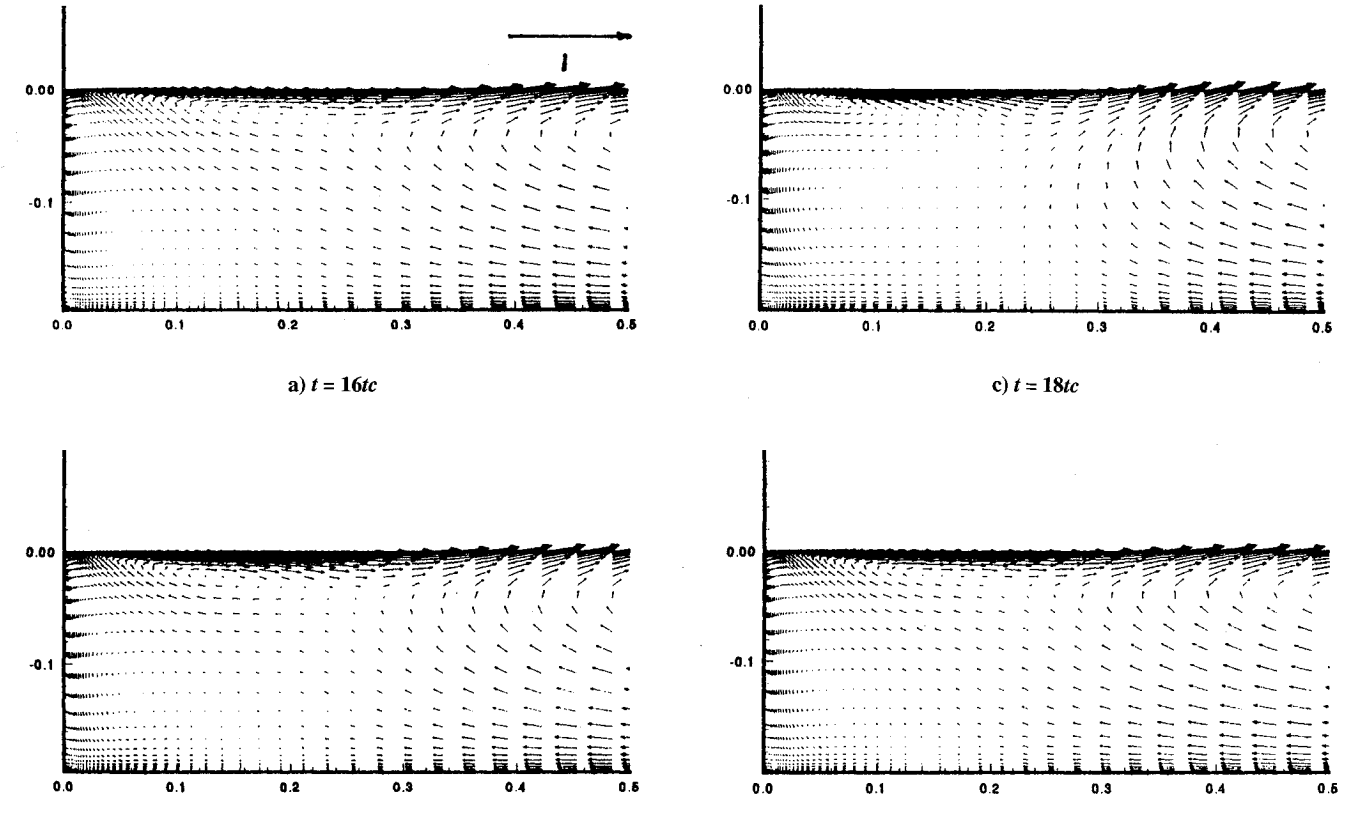

a) $t = 16tc$

c) $t = 18tc$

b) $t = 17tc$

d) $t = 19tc$

Fig. 4 Instantaneous velocity vectors near the forward bulkhead.

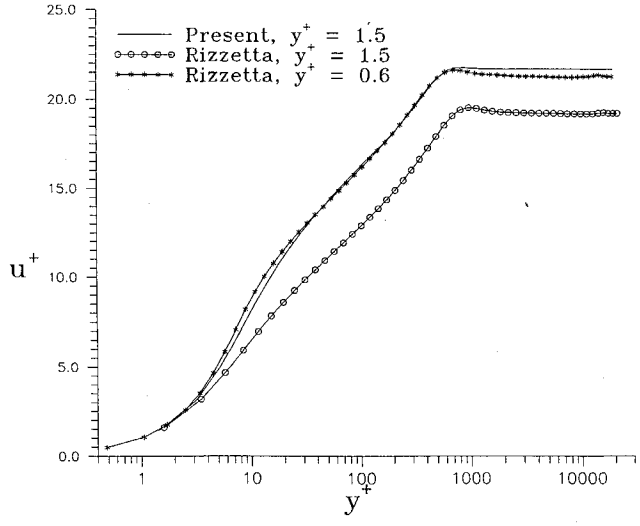

Fig. 5 Incoming boundary layer at $X/L = -0.19916$.

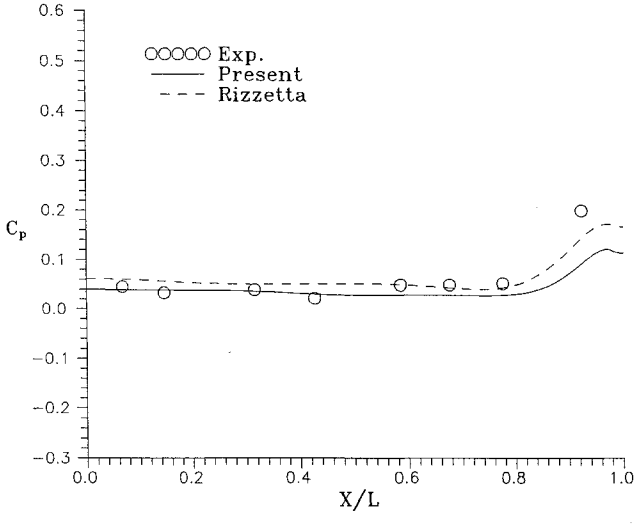

Fig. 6 Mean static pressure distribution along the cavity floor.

resulting in a series of compression and expansion waves both within the cavity and in the external flow. Figures 2a and 3a indicate the compression wave at the aft bulkhead, the shear layer bulges outward, and mass is ejected out of the cavity. After the shear layer reattaches at the aft bulkhead, the mass addition creates a traveling pressure wave that moves forward in the cavity, trailing an oblique shock in the freestream at $x = 0.2$ as one can see in Figs. 2b and 3b. When the traveling pressure wave reaches the forward bulkhead and reflects, a pressure doubling occurs in the cavity whereas disturbances in the external flow are not reflected, and thus a pressure jump across the shear layer deflects the shear layer at $x = 0.4$ as one can see in Figs. 2c and 3c. Also, the pressure wave impacts the forward bulkhead and produces a stronger compression wave emanating from the upstream corner of the cavity. Figures 2d and 3d show that the reflected pressure wave in the cavity moves downstream, deflects the shear layer outward at the aft bulkhead, and the compression wave at the upstream corner of cavity becomes weaker and leaves the upstream corner of cavity. The alternating sequence of compressions and expansions produced by the waviness of the shear layer is evident.

Instantaneous velocity vectors near the forward bulkhead at corresponding time levels are presented in Fig. 4. The purpose of these figures is to indicate the generation of vortices that occurs at the forward cavity lip and its convection downstream. Figure 4b shows a large vortex near the center of cavity ($x = 0.5$), and a small vortex at $x = 0.14$, generated previously at the forward cavity lip (recall that the forward traveling pressure wave is at $x = 0.2$ at this time, Fig. 3b). The small vortex moves downstream and emerges with the large vortex. When the forward traveling wave reflects from the forward bulkhead, a vortex is generated at the forward cavity lip as one can see in Fig. 4c at $x = 0.05$. The periodic shedding of vortices from the lip of the forward bulkhead is observed repeatedly throughout the oscillation cycle, which verifies the simple physical model suggested by Rossiter.[2]

Figures 6–9 present the computed mean static and acoustic pressure distributions over the cavity surfaces that are compared with the experimental data of Kaufman et al.[1] Also shown in the same figures are computed results that were obtained using Rizzetta's code[14] in which a subiteration technique is used in the solution of the uncoupled k-ε equations. That code required finer grid to achieve similarity with our computed velocity profile at 0.19916 times the cavity length upstream of the cavity forward bulkhead. Figure 5 compares the computed profiles for the two codes with the same grid with the first grid point at $y^+ = 1.5$ as well as the one obtained from Rizzetta's code with a finer grid ($y^+ = 0.6$). Based on this, a 150×61 grid was used on and above the plane of the cavity mouth, and 96×60 grid inside the cavity was used with Rizzetta's code. The time step size had to be reduced to 1.25×10^{-4} and three subiterations were employed. The entire calculation required 30 CPU h on the Cray Y-MP.

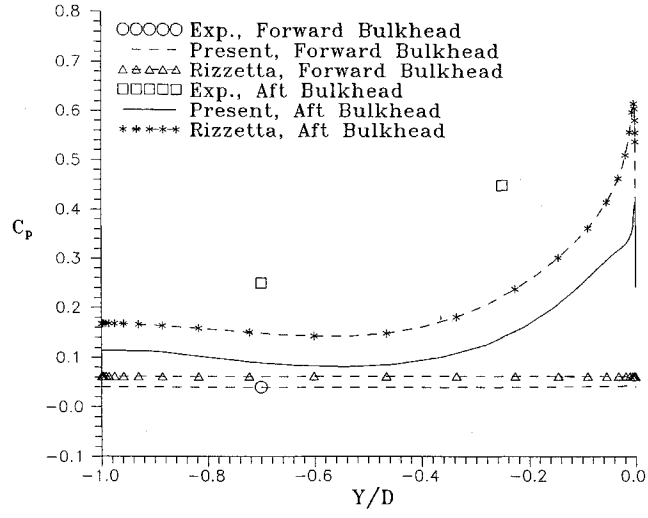

Fig. 7 Mean static pressure distribution along the forward and aft bulkheads.

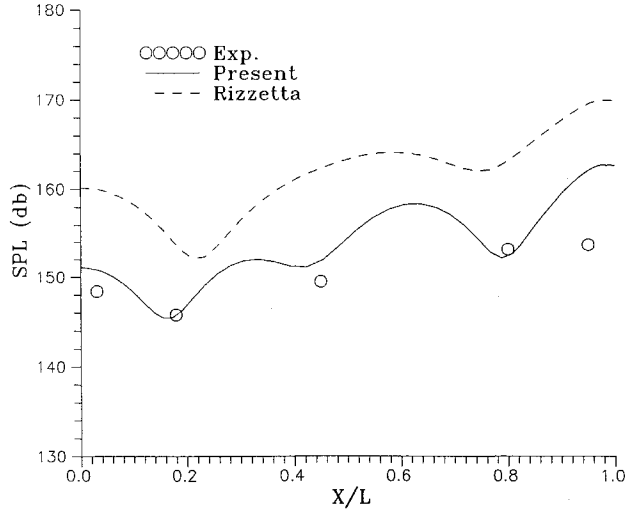

Fig. 8 Overall sound pressure level distribution along the cavity floor.

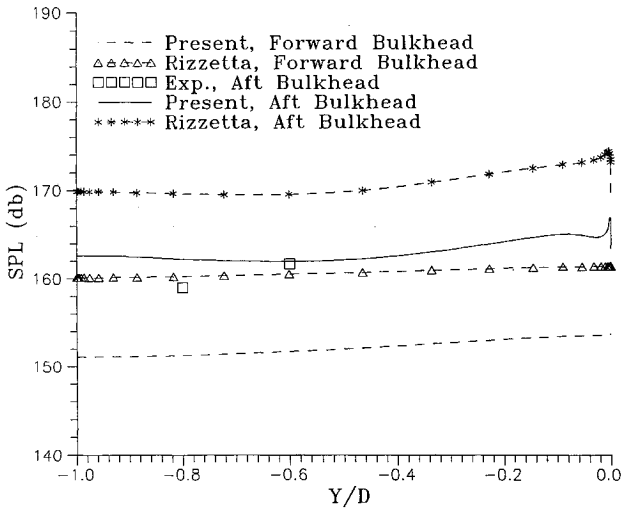

Fig. 9 Overall sound pressure level distribution along the forward and aft bulkheads.

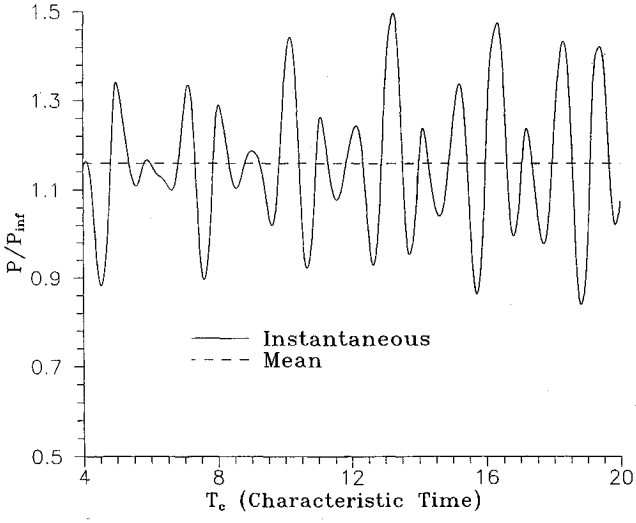

Fig. 10 Pressure time history on the aft bulkhead at $y/D = -0.4$.

Figure 6 presents the mean static pressure distribution along the cavity floor. Here the static pressure coefficient C_p is defined as

$$C_p = \frac{2(\bar{p} - p_\infty)}{\rho_\infty u_\infty^2}, \qquad \bar{p} = \frac{1}{(t_f - t_i)} \int_{t_i}^{t_f} p \, dt \tag{12}$$

The pressure distribution is seen to be relatively constant over the first 80% of the length of the cavity and then rises sharply near the aft bulkhead. The computations agree very well with the experimental data upstream of the midcavity and underpredict the pressure level downstream. The present code predicts a mean static pressure level less than that of Rizzetta's code. Figure 7 displays the corresponding mean static pressure distributions on the forward and aft bulkheads. At the forward bulkhead, the present code predicts exactly the pressure level that is virtually constant along the forward bulkhead, whereas Rizzetta's code slightly overpredicts it. At the aft bulkhead, both codes underpredict the mean static pressure level with the results obtained from Rizzetta's code closer to the experimental data. Consistent with Fig. 6, the computational result underpredicts the pressure downstream. The differences between the numerical solution and experimental data are notable on the rear bulkhead where the pressure fluctuations are higher. The reasons for the differences are attributed to three-dimensional effects and excessive viscous dissipation in the k-ε model. Rizzetta[5] compared the two- and three-dimensional computations using algebraic turbulence model with the experimental data and found that the three-dimensional computations predicted higher pressure level near the rear bulkhead. Rizzetta and Visbal[14] performed the numerical simulations of airfoil dynamic stall using algebraic and k-ε turbulence models. They found that high peak values of the force coefficients were not predicted in the case of k-ε model due to the excessive viscous dissipation produced in the equations.

In Fig. 8, the acoustic pressure distribution along the cavity floor is represented as overall sound pressure level SPL, in decibels, which is defined as follows:

$$\text{SPL} = 10 \log_{10}(\bar{p}^2/q^2), \qquad \bar{p}^2 = \frac{1}{(t_f - t_i)} \int_{t_i}^{t_f} (p - \bar{p})^2 \, dt \tag{13}$$

where q is the acoustic sound reference level of 2×10^{-5} Pa. The computed results of the present code agrees with the experimental data except near the rear bulkhead. Rizzetta's code predicts 10 db higher sound pressure level than that of experimental measurements. Figure 9 presents the corresponding overall sound pressure levels along the forward and aft bulkheads. Slight difference between the present computed results and experimental data can be seen near the floor of the cavity at the rear bulkhead. Rizzetta's code again predicts 10 db higher sound pressure level than that of the experimental data. As expected, the aft bulkhead experiences a 10–15 dB higher SPL than does the forward bulkhead.

The time history of the fluctuating pressure obtained from the present code on the rear bulkhead at $y/D = -0.4$ is displayed in Fig. 10. For comparison, the mean pressure level is also indicated. It can be observed that although the mean pressure value is only about 16% higher than freestream value, peak levels can be as much as 1.5 times freestream static pressure. Based on the experimental data,[1] the first harmonic of the oscillation is approximately 1 kHz, which agrees with the spacing between major pressure peaks of $\Delta T_c = 3.5$ in Fig. 10, which is approximately 10^{-3} s.

Conclusions

A numerical solution procedure was developed for the simultaneous implicit numerical solution of the strongly coupled k-ε and compressible Navier-Stokes equations without the application of the subiteration technique. With the proposed damping terms, the present algorithm is shown to enhance the stability (larger time step size) and relieve the stiffness associated with the solution to k-ε equations. The results are presented for the simulation of unsteady supersonic flow over an open cavity at a freestream Mach number of 1.5 and Reynolds number of 1.09×10^6. Throughout the oscillation cycle, the periodic shedding of vortices from the lip of the forward bulkhead and the shear-layer deflection due to the pressure waves traveling upstream and downstream were observed, verifying the physical mechanism envisioned by the experimentalists. Quantitative comparisons are made with the experimental data for the mean static pressure and overall acoustic sound pressure level within the cavity. Although the present code underpredicts the mean static pressure level near the aft bulkhead, the overall sound pressure levels including the first harmonic of the oscillation, which is approximately 1 kHz, are well predicted.

Acknowledgments

This work was sponsored by AFOSR Contract 91-0101 with L. Sakell as project monitor. The computational work was performed on the Cray Y-MP of the Ohio Supercomputer Center.

References

[1]Kaufman, L. G., II, Maciulaitis, A., and Clark, R. L., "Mach 0.6 to 3.0 Flows over Rectangular Cavities," Air Force Wright Aeronautical Labs., AFWAL-TR-82-3112, May 1983.

[2]Rossiter, J. E., "Wind Tunnel Measurements on the Flow over Rectangular Cavities at Subsonic and Transonic Speeds," Ministry of Aviation, Aeronautical Research Council, R&M 3438, London, Oct. 1964.

[3]Borland, C. J., "Numerical Prediction of the Unsteady Flowfield in an Open Cavity," AIAA Paper 77-673, June 1977.

[4]Hankey, W. L., and Shang, J. S., "Analyses of Pressure Oscillations in

an Open Cavity," *AIAA Journal,* Vol. 18, No. 8, 1980, pp. 892–898.
[5]Rizzetta, D. P., "Numerical Simulation of Supersonic Flow Over a Three-Dimensional Cavity," *AIAA Journal,* Vol. 26, No. 7, 1988, pp. 799–807.
[6]Hankey, W. L., and Calarese, W., "Reynolds Stresses for Unsteady Turbulent Flows," *AIAA Journal,* Vol. 21, No. 8, 1983, pp. 1210, 1211.
[7]Rubesin, M. W., "Turbulence Modeling for Aerodynamic Flows," AIAA Paper 89-0606, Jan. 1989.
[8]Coakley, T. J., and Huang, P. G., "Turbulence Modeling for High Speed Flows," AIAA Paper 92-0436, Jan. 1992.
[9]Sahu, J., and Danberg, J. E., "Navier-Stokes Computations of Transonic Flows with a Two-Equation Turbulence Model," *AIAA Journal,* Vol. 24, No. 11, 1986, pp. 1744–1751.
[10]Coakley, T. J., "Turbulence Modeling Methods for the Compressible Navier-Stokes Equations," AIAA Paper 83-1693, July 1983.
[11]Chien, K.-Y., "Predictions of Channel and Boundary-Layer Flows with a Low-Reynolds-Number Turbulence Model," *AIAA Journal,* Vol. 20, No. 1, 1982, pp. 33–38.
[12]Nichols, R. H., "A Two-Equation Model for Compressible Flows," AIAA Paper 90-0494, Jan. 1990.
[13]Cooper, G. K., and Sirbaugh, J. R., "PARC Code: Theory and Usage," Arnold Engineering Development Center, AEDC-TR-89-15, Dec. 1989.
[14]Rizzetta, D. P., and Visbal, M. R., "Comparative Numerical Study of Two Turbulence Models for Airfoil Static and Dynamic Stall," AIAA Paper 92-4649, Aug. 1992.
[15]Shih, S. H., "Implicit Procedure for the Solution of the Unsteady Coupled k-ε and Navier-Stokes Equations," Ph.D. Dissertation, Dept. of Aerospace and Engineering and Engineering Mechanics, Univ. of Cincinnati, Cincinnati, OH, June 1993.
[16]Beam, R., and Warming, R., "An Implicit Factored Scheme for the Compressible Navier-Stokes Equations," *AIAA Journal,* Vol. 16, No. 4, 1978, pp. 393–402.